Applied Ocean Research 78 (2018) 212–222

Contents lists available at ScienceDirect

Applied Ocean Research

journal homepage: www.elsevier.com/locate/apor

Effects of operating parameters and injection method on the performance of an artificial upwelling by using airlift pump

Yongfa Qiang[a], Wei Fan[a,*], Canbo Xiao[a], Yiwen Pan[a], Ying Chen[b]

[a] Ocean College, Zhejiang Univ., Zhoushan, 316021, China
[b] Ocean College and State Key Laboratory of Fluid Power & Mechatronic System, Zhejiang Univ., Hangzhou, 310027, China

ARTICLE INFO

Keywords:
Airlift pump
Artificial upwelling
Injection method
Operating parameters
Lift effectiveness

ABSTRACT

Artificial upwelling by using airlift pump is considered a sustainable way in actualizing ocean fertilization, which could potentially alleviate the pressures on the fish stocks and human-driven climate change. However, few experimental data about the effects of operating parameters and injection method on the performance of the airlift artificial upwelling were found in the literature. In this paper, an airlift pump for artificial upwelling was investigated through three field experiments, in which airlift pumps of pipe length ranges from 20 to 28.3 m and pipe diameter ranges from 0.4 to 2 m, were designed and tested. Pumped water flow rate and injected air flow rate were measured to study the effects of different factors on the performance of airlift pump. The experiment results show that airlift pump efficiency is closely related to pipe diameter, submerged depth, submergence ratio and nozzle designs. There is no best nozzle for all the range of air flow rate, and the recommended nozzles are double-ring-shaped or star-shaped nozzles when the air flow rate is less or more than 220 L/min, respectively. Moreover, the lift effectiveness increases when the hole size of nozzle is enlarged, which indicates a relatively large bubble size will enhance the lift effectiveness.

1. Introduction

Deep ocean water (DOW), which is deeper than 200 m, has high nutrient concentration as compared to epipelagic seawater [1]. The nitrate, phosphate and other nutrients dissolved in the DOW constitute the raw materials for plant growth. Thus primary productivity could be enhanced by artificially upwelling the nutrient-rich DOW to the surface, feeding the phytoplankton, and further increasing organic carbon exportation to the deep ocean via the biological pump and the microbial pump [2]. Though natural upwelling occurs over about 0.1% of the ocean and produces about 44% of the world's fish catch [3], it is hard to be utilized for its seasonality and locality. Unlike the natural upwelling, the artificial upwelling is not seasonal and regional, and can be applied in many parts of the world [2,4].

The research on artificial upwelling over the past few decades has generated various types of artificial upwelling such as the perpetual salt fountain [5–7], the wave-powered pump [8–10] and the airlift pump [4,11]. The perpetual salt fountain does not need any artificial power source to upwell deep sea water. However, the flow rate with a single pipe was estimated approximately 45m^3/day, which is too small to benefit the phytoplankton [7]. If such an artificial upwelling were to be viable for an ocean farming project, a large number of upwelling pipes would be necessary [12]. Compared with the salt fountain, the estimated flow rate of the wave-powered pump is about 38,000–82,000 m^3/day for a 1.90 m wave height and 12-sec wave period [13]. But the stiff long pipe of wave-powered pump may not survive in a storm wave [11].

The type of airlift pump injects a gas, usually air, in the lower part of a pipe that transports the liquid. As a result of the gas bubbles suspended in the water, the average density of the two-phase mixture in the pipe is less than that of the surrounding fluid. By fluid pressure, the liquid is taken in the ascendant air flow and moves in the same direction as the air [4]. The airlift pump have several advantages, i.e., large seawater flow rate, lower initial and maintenance costs, easy installation and flow rate regulation. These advantages, accompanied by the simplicity and lack of moving mechanical parts, meaning that airlift pumps can be used for pumping hydrocarbons, dirty water, dangerous and noxious fluids [14,15], seabed mining [16], and cold, nutrient-rich DOW in a sustainable way [4,11,17].

For the conventional airlift pumps which are devices lifting water through a vertical pipe partially submerged in the water, some studies on the injection method of airlift pumps have been conducted in the laboratory [18,19]. Khalil, Elshorbagy [20] experimentally investigated the performance of an airlift pump using different injection disks at different submergence ratios (the ratio between the immersed length of

* Corresponding author.
E-mail address: wayfan@zju.edu.cn (W. Fan).

https://doi.org/10.1016/j.apor.2018.06.006
Received 27 February 2018; Received in revised form 31 May 2018; Accepted 5 June 2018
Available online 30 June 2018

the pipe and its total length). In the experiments, they found that there is a suitable disk design for maximum water flow rate and the highest efficiency resulted at the largest submergence ratio. Ahmed, Aman [21] studied the airlift pump with different air injectors to enable injection radially, axially, dual and swirl. Experiment results have shown that dual injection outperformed the other injections because of its high efficiency over the entire range of air mass flow rate.

Unlike the conventional airlift pumps, the airlift pump for artificial upwelling of deep water, is operated in a totally submerged mode [4]. Thus, the injection methods and some definitions such as submergence ratio are different from the conventional ones. Liang and Peng [11] described a conceptual airlift pump for upwelling deep ocean water through a vertical pipe which totally submerged in the seawater, and by compressing air into the pipe near the upper end. Fan, Chen [4] and Yang, Zhang [22] tested the feasibility and stability of the injection method proposed by Liang and Peng [11] in the field experiments. The pumped water flow rate is about 300 m^3/h at an air flow rate of 30 m^3/h, proving this kind of airlift pump to be a feasible and effective way for upwelling DOW. However, few experimental data about the influence of operating parameters and injection method on the performance of the airlift artificial upwelling were found in the literature. To investigate the influence of operating parameters and injection method, such as diameter and submerged depth (the depth where the upper end of upwelling pipe below the water surface) of the upwelling pipe, submergence ratios and different designs of the nozzle, the authors have performed several field experiments of airlift pumping system both in the lake and the sea.

This paper is organized as follows. First, the experimental setup of an airlift artificial upwelling is proposed, and then the sites, seasons and process of two lake experiments and an open ocean trial are described. Next, the experiment results and the analysis are given respectively. Finally, some conclusions are summarized.

2. Experimental setup

2.1. Artificial upwelling system design

Fig. 1 shows the schematic of the airlift pump system for artificial upwelling in the field experiments. The artificial upwelling system mainly consists of the upwelling pipe, the air compressor, the air supply pipes and an engineering ship. The power for upwelling was provided by the engineering ship, on which there was a crane to help hanging the upwelling pipe in the water. The upwelling pipe was totally submerged in water and it was divided into two parts by the depth of injection nozzle, the water suction section (below the nozzle) and the air injection section (above the nozzle). In the suction section, there was only water flowing, while all of the air injection section was occupied by the air-water two-phase flow. Pipes of different lengths and diameters were tested in the experiments, and to accommodate different experimental environments, pipe materials of nylon-reinforced PVC sheet and iron sheet were used in lake and sea trial experiments, respectively. The details of upwelling pipes in each experiment are listed in Table 1.

In order to study the effect of submergence ratio, there were several depths available to fix the nozzles at the upper pipe (See Fig. 1). At each fixing depth, a cross-shaped steel shelf was welded to the upwelling pipe, and nozzles were fixed to the steel shelf by cable ties. For every nozzle in the upwelling pipe, its injection port was connected with the air supply pipe (16 mm inner diameter), through which the air was supplied continually by an air compressor (JBao3540). To allow only one nozzle injecting air at a time in the experiment, the supplied air was switched by a four-way directional valve after coming out of the air compressor (See Fig. 1). To directly observe the volume flow rate of upwelled water, a tracing system consisting of the tracer solution, submersible pump, underwater camera and water pipe was used. The potassium permanganate solution was selected as the tracer and was kept in the tracer tank. A submersible pump was used to inject the tracer to the bottom through a water pipe, which connected the tracer tank and the lower end of the upwelling pipe.

2.2. Operating parameters and injection method

Operating parameters investigated here includes pipe diameter, submerged depth and submergence ratio. Different from the conventional airlift pumps which are partially submerged in the water, the airlift pump for artificial upwelling is totally submerged in the water. Therefore the definition of submergence ratio (SR) is different from the conventional airlift pumps, and here it denotes the ratio between the

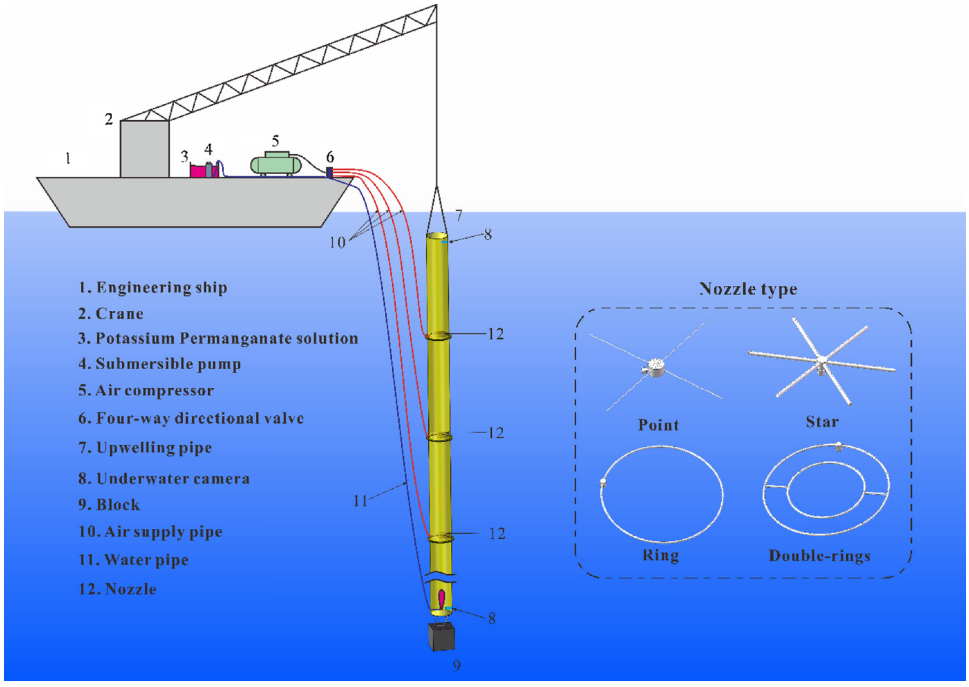

Fig. 1. The schematic of the airlift pump system for artificial upwelling.

Table 1
Details of experiment sites and equipment used in every experiment.

Exp.	Time	Location	Length	Diameter	Material	Nozzles[a]
Lake 1	Sep. 2012	29°33′51″N, 119°11′9″ E	28.3 (m)	0.4 (m)	Nylon- reinforced PVC	R1, R4
Lake 2	Dec. 2012	29°33′51″N, 119°11′9″ E	26 (m)	0.5, 1, 1.5, 2 (m)	Nylon-reinforced PVC	P1, P3, S2, S4, R2, R4, D1, D2
Sea trial	Sep. 2014	30°8′14″ N, 122°44′59″ E	20(m)	0.4 (m)	Iron	P2, P3, S1, S3, S4, R1, R3, R4

[a] The type of nozzles can be found in Table 2.

injection depth to the upper end of upwelling pipe and the total upwelling pipe length [4]. In the experiments, upwelling pipe of different diameters (0.4, 0.5, 1, 1.5, and 2 m, See Table 1) were used at different submergence ratios (0.125, 0.25, 0.28, 0.32 and 0.375) with different submerged depths (0.15, 1, 2.3 and 3 m). The detailed experiment conditions can be found in Table A1 in the Appendix.

The designs of injection method includes the shape and hole size of nozzle designed. Figs. 1 and 2 show the nozzles of different types used in the experiments, in which there are a total of four different types, point, star, ring, and double-rings. The nozzles were made of stainless steel block or tubes with different processing techniques, and they had many injection holes that are evenly distributed on them. The holes were drilled into the steel block or tubes through plasma arc drilling. For point type, the nozzle was made of a hollow steel block with four slender steel bars to fix in the upwelling pipe, and the injection holes were evenly distributed on the upper surface of the block. For star type, the nozzle was made of steel tubes with one end was closed and the other ends were welded together (see Fig. 2), and the inner diameter of the steel tube was 8 mm. The injection holes were designed to distribute evenly on the upper surface of each steel tube. For ring and double-tings type, the nozzle was made by bending the steel tube into ring, and the injection holes were evenly distributed on the upper surface of the rings. At each fixing depth, the upwelling pipe had a cross-shaped shelf to fix the nozzle. The nozzle was placed inside the upwelling pipe and at the center of the pipe transverse to reduce the collision with the pipe wall. Each nozzle had a hexagonal port to connect with the air supply pipe and thus connecting with the air compressor. In the experiments, a total of 15 nozzles were used (See Table 2). All the nozzles had a same total hole area of 75.4 mm^2 to make sure the total injection area was the same for every experiments. Holes with different diameters (0.5, 1, 1.5 and 2 mm) and different numbers (24, 42, 96 and 384) were designed, and the specifications of holes on each nozzle are listed in Table 2.

2.3. Experiment sites and seasons

A total of three experiments in different sites and seasons were conducted in this study, including two lake experiments and one open sea trial (See Fig. 3).

The lake experiments were conducted in Qiandao lake, Chuan'an County, Zhejiang Province, China, with the north latitude 29°33′51″ and east longitude 119°11′9″ (Fig. 3b). The first one was carried out in September 2011, at the end of summer when the lake water was well-stratified. The vertical distribution of temperature and density in the first lake experiment is shown in Fig. 4a, which was measured by the

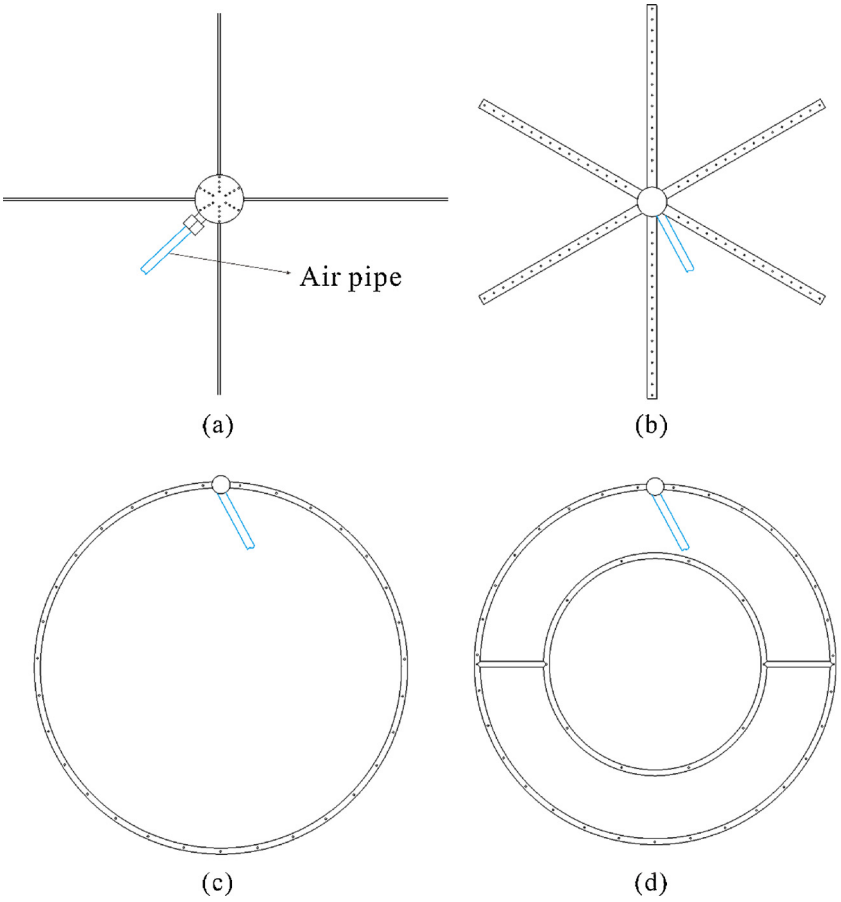

Fig. 2. Schematic of different nozzle types. (a) Point type; (b) Star type; (c) Ring type; (d) Double-rings type.

Table 2
Different air injection nozzles used in the experiments.

Nozzle shape	Nozzle No.	Number of holes	Hole diameter (mm)	Total area of holes (mm^2)
Point	P1	42	1.5	75.4
	P2	96	1	75.4
	P3	384	0.5	75.4
Star	S1	24	2	75.4
	S2	42	1.5	75.4
	S3	96	1	75.4
	S4	384	0.5	75.4
Ring	R1	24	2	75.4
	R2	42	1.5	75.4
	R3	96	1	75.4
	R4	384	0.5	75.4
Double-rings	D1	42	1.5	75.4
	D2	384	0.5	75.4

conductivity-temperature-depth recorder (CTD, SST CTD48 M). The thermocline which is between the mixed layer and the cold lower layer of water, was at about 17–31 m in the lake. The temperature of the lake water ranged from 14.2 to 22.2 ℃, and the density of the lake water ranged from 997.79 to 999.40 kg/m^3. Hence, the maximum density difference was 1.61 kg/m^3. To test the airlift pump in a less-stratified water environment, a second experiment was conducted in winter in December 2012. Fig. 4b presents the measured vertical distribution of temperature and density of the second lake experiment. The thermocline was near 26 m, and the temperature of the lake water ranged from 10.3 to 16.0 ℃, much colder than that in the first lake experiment. The density ranged from 998.92 to 999.68 kg/m^3 and hence the maximum density difference was 0.76 kg/m^3. Details of experiment sites and conducted seasons for every experiment are list in Table 1.

The open sea trial was conducted in the East China Sea near Dongji island (30°8′14″ N, 122°44′59″ E) in September 2014 (Fig. 3c). Fig. 4c shows the measured vertical distribution of temperature, salinity and density, respectively. The thermocline interface was at about 17 m, and to upwell nutrient-rich deep cold water to the upper layer, the bottom of upwelling pipe was set at 21 ~ 23 m below the sea surface. The density difference between the water of 23 m deep and the surface is 8 kg/m^3.

2.4. Experiment process

In the experiment, the upwelling pipe was deployed from the engineering ship after the air supply pipes were connected to the nozzles and the air compressor. Then, the upwelling pipe was hanged in the water by the crane, and kept straight against the horizontal flow by the weight at its bottom end. When the upwelling pipe became steady in the water, the air was injected to the nozzle through air supply pipes, and volume flow rate of air was measured by gas flowmeter (MF5612). Next, after the bubbles continuously rose to the water surface, the submersible pump began to inject the tracer to the bottom of upwelling pipe through the water pipe, and the time the tracer arrived at the bottom was determined by the underwater camera. Thus the mean volume flux can be approximately obtained by measuring the time the tracer took to move from the lower end of upwelling pipe to the top end of upwelling pipe. Some typical photos of artificial upwelling in the experiments are presented in Fig. 5.

3. Results and discussion

3.1. Effects of pipe diameter on pumped water flow rate

Lake experiments 2–1, 2–4, 2–12 and 2–16 are selected to study the effects of pipe diameter on pumped water flow rate, and the results of lifting cold and dense water with different pipe diameters are presented in Fig. 6. The pumped water volume flow rate versus the injected air volume flow rate is plotted as different symbols to represent pipe diameters of 0.5, 1, 1.5 and 2 m. Experiments in Fig. 6 were conducted at the same air injection conditions, and the injection nozzle shape is point, with 1.5 mm hole size and 42 holes in total. The submerged depth were 1.7 and 2 m for lake experiments 2–1, 2–4 and 2–12, 2–16, respectively. According to the vertical profile of density in lake experiment 2 (see Fig. 4b), the density difference of sucked water (near the lower end of upwelling pipe) caused by the gap of 0.3 m in depth is limited (less than 0.1 kg/m^3), and can be negligible compared to the influence caused by pipe diameter. Thus the experiments in Fig. 6 are approximately treated to be done at the same submerged depth. Besides, in order to eliminate the influence caused by relative scale of nozzle diameter to the pipe diameter, the nozzle size are selected according to the upwelling pipe diameter in Fig. 6 to make the relative scale approximately the same. Therefore, experiments in Fig. 6 are approximately considered to be conducted under the same conditions except for the pipe diameter. From Fig. 6, when the injected air flow rate is lower than 25 L/min, there is no significant differences of pumped water flow rate between upwelling pipes of different diameters. As the injected air flow rate increases, the difference of pumped water flow rate between upwelling pipe of 1 m and 2 m becomes obvious, while the pipe of diameter 0.5 m and 1.5 m almost keeps the same trend. Pipe of diameter 1 m pumps much more water over the other three pipes at the same air volume flow rate, and the next best is

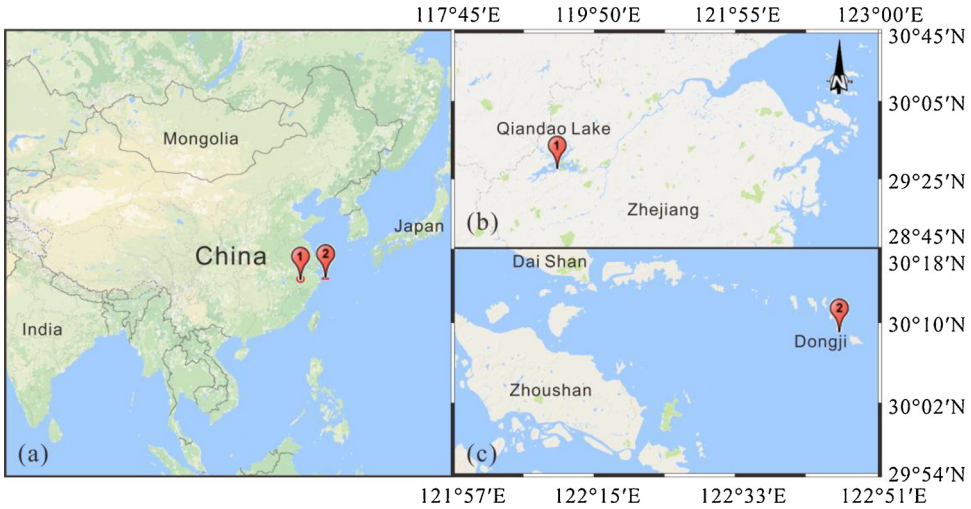

Fig. 3. Experiment sites. (a) Overview of two experiment sites; (b) Experiment in Qiandao lake; (c) Sea trial near Dongji island.

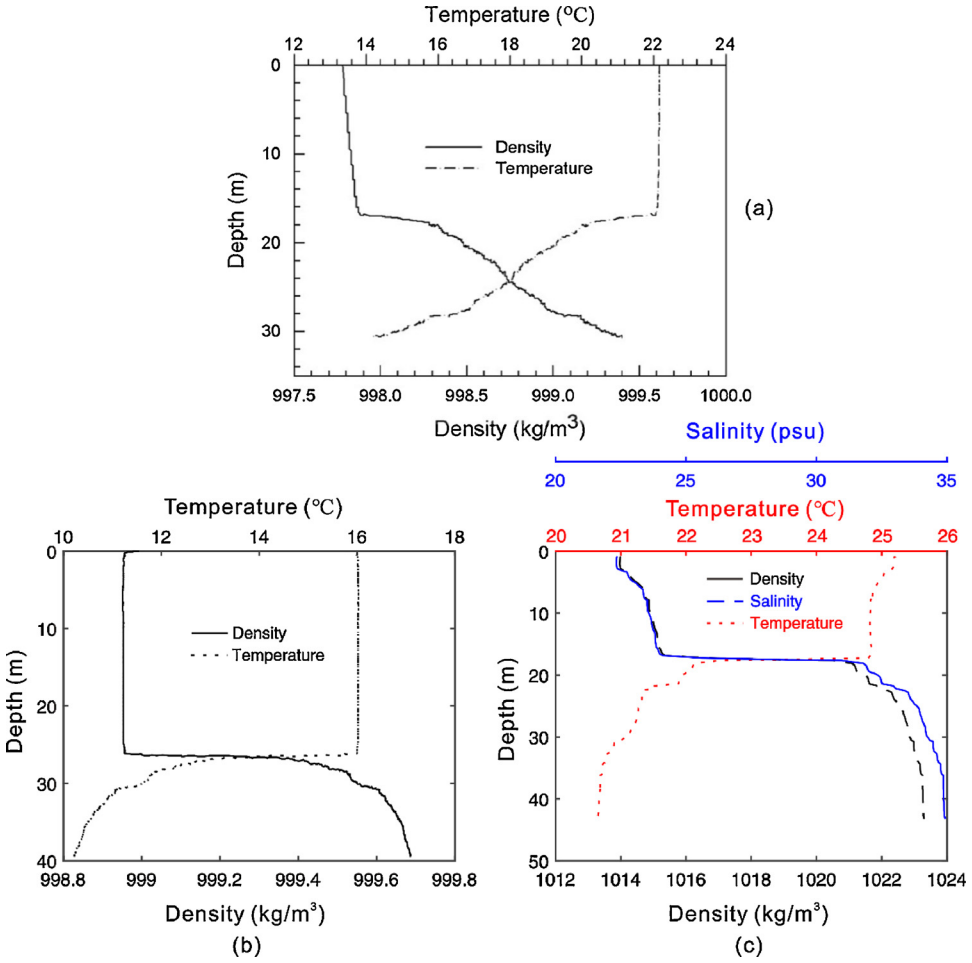

Fig. 4. Vertical distribution of temperature and density at the experiment location. (a) Lake experiment 1; (b) Lake experiment 2; (c) Sea trial.

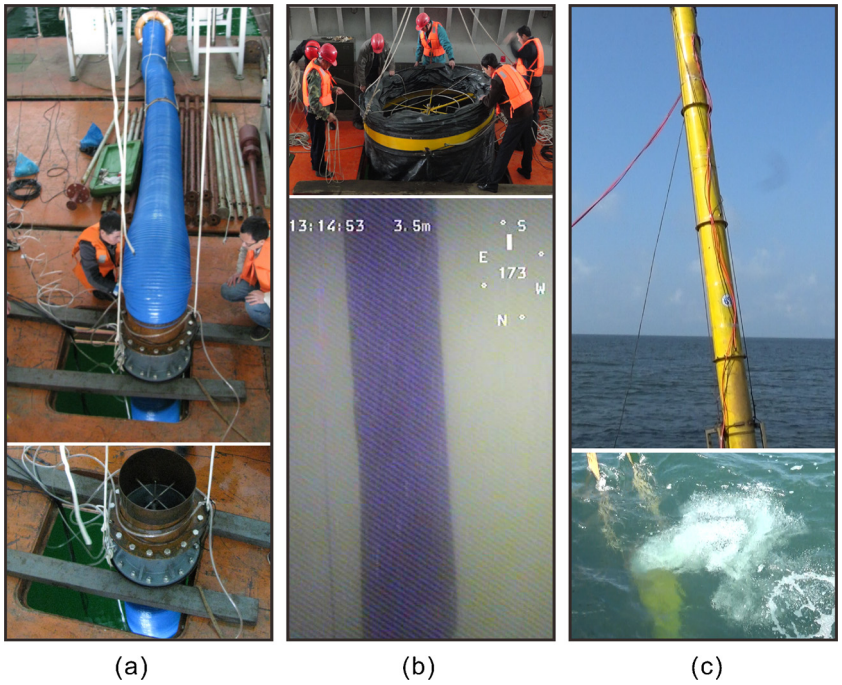

Fig. 5. Photos of artificial upwelling in the experiments. (a), (b) Lake experiments 1 and 2 in Qiandao Lake; (c) The sea trial near Dongji island.

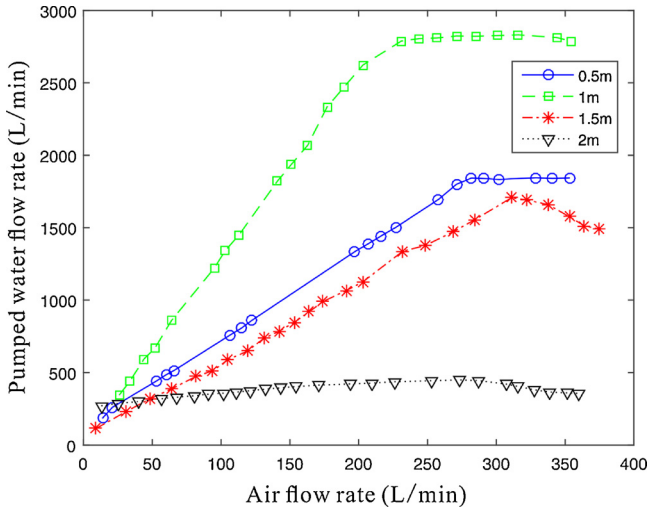

Fig. 6. Variations of pumped water volume flow rate versus air volume flow rate for different upwelling pipe diameters (Lake 2–1, 2–4, 2–12, 2–16).

pipe of diameter 0.5 m, which is slightly more than the pipe of diameter 1.5 m. The last to recommend is pipe of diameter 2 m, which stays almost the same as the air volume flow rate changes. Furthermore, as the injected air flow rate keeps increasing, the increasing rate of pumped water slows down and even drops, which means continuing to increase the injected air volume flow rate will cause increase in pumped water volume flow rate, but at a cost of reducing airlift efficiency. In order to obtain a dimensionless parameter for the airlift pump efficiency without considering the pressure loss caused by devices and blockages such as nozzle, valves, pipe bends and contractions, and thus to compare the performances of airlift pumps of different designs, a suitable parameter is the lift effectiveness, which denotes the ratio between the volume flow rate of pumped water and the injected air.

Fig. 7 shows the lift effectiveness of airlift ratio between the volume flow rate of pumped water and injected air, in which it can be clearly seen that the higher injected air volume flow rate leads to a higher pumped water volume flow rate and also a lower lift effectiveness. If the injected air flow rate increases further, it will result in a dramatic reduction in lift ratio. For upwelling pipe of diameter 2 m, the lift effectiveness even reduces to 1 when the injected air volume flow rate is about 350 L/min.

From Figs. 6 and 7, it can be seen that pipe of diameter 1 m performs best among the four diameters. Two main factors account for this result,

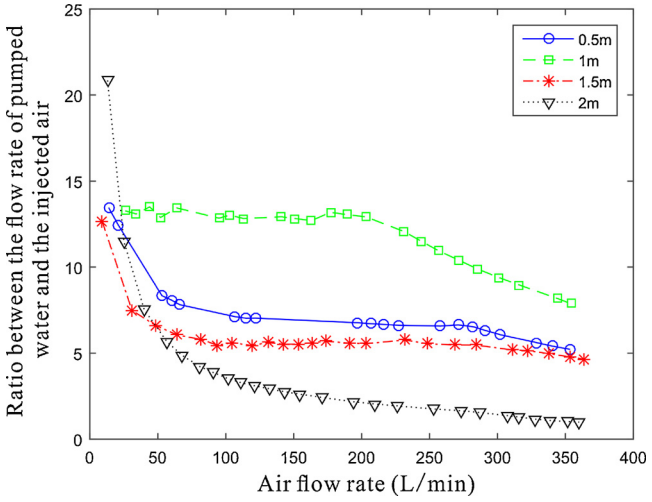

Fig. 7. Variations of lift effectiveness for different pipe diameters (Lake 2–1, 2–4, 2–12, 2–16).

the friction loss on the pipe inner wall and the effective injection area of supplied air. When the pipe diameter is less than 1 m, the effect of friction loss on the lift effectiveness is relatively larger than that of effective injection area, and an increase of pipe diameter results in a smaller friction loss and a higher lift effectiveness. On the other hand, when the pipe diameter is more than 1 m, the effect of effective injection area is greater than that of friction loss. An increase of pipe diameter leads to a smaller effective injection area that produces less lift force for ambient water and even causes M-shaped flow in the pipe, thus leading to a lower lift effectiveness in the end. Therefore, it seems that the lift effectiveness of upwelling increases with the increase of the upwelling pipe diameter first (from 0.5 m to 1 m), and then it decreases as the pipe diameter keeps increasing (from 1 m to 2 m). Hence in this study, upwelling pipe of diameter 1 m has the highest lift effectiveness among the four diameters, and the effectiveness ranges from 7 to 14 when air flow rate ranges from 50 to 350 L/min/.

3.2. Effects of submerged depth on pumped water flow rate

Fig. 8 presents the experiment results of pumped water flow rate at different submerged depths of 0.15 m and 2.3 m. For both submerged depths, it is clear that the pumped water volume flow rate increases with the increase of injected air volume flow rate, and the growth rate slows down after an air flow rate of 200 L/min. When air flow rate is below 50 L/min, there is no significant difference between the two submerged depths. However, the difference becomes obvious as the air flow rate keeps increasing. When the supplied air flow rate is below 400 L/min, the maximum pumped water flow rate is about 4800 L/min and 2800 L/min for upwelling pipe deployed at 0.15 m and 2.3 m underwater, respectively. From Fig. 8, it can also be seen that the lift effectiveness increases at first, and then decreases with the increase of air flow rate after it reaches the maximum value. For both submerged depths, the lift effectiveness remains above 10 when the air flow rate is less than 300 L/min. For upwelling pipe deployed at 2.3 m, the pumped water flow rate reaches a maximum lift effectiveness of 18 when the air flow rate is about 75 L/min. For upwelling pipe deployed at 0.15 m, the maximum lift effectiveness is around 27, and it occurs at an air flow rate of 125 L/min.

Fig. 9 is the experiment results of pumped water flow rate at different submerged depths from the sea trial 1–6 and 1–9. The results indicate that a very low air flow rate can not pump water from the bottom due to a high water density difference between the lower and the upper ends of the pipe, which can be more than 8 kg/m^3 (see Fig. 4c). In order to achieve the upwelling of water, a minimum air flow

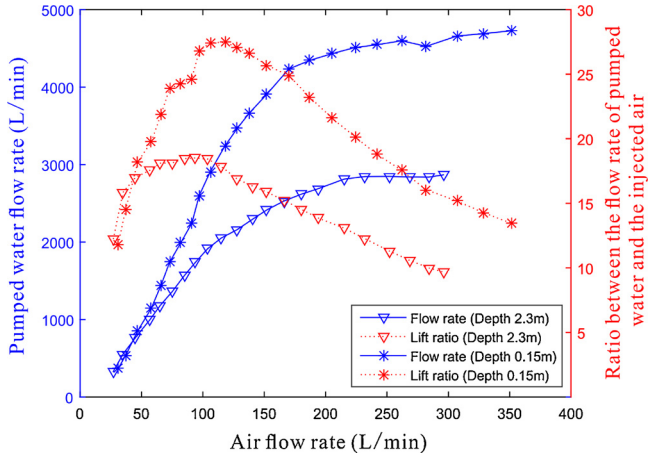

Fig. 8. Variations of pumped water volume flow rate and lift effectiveness at different submerged depths (Lake experiments 2–5 and 2–6). The triangles and the axes stand for pumped water flow rate at submerged depths of 2.3 m and 0.15 m, respectively.

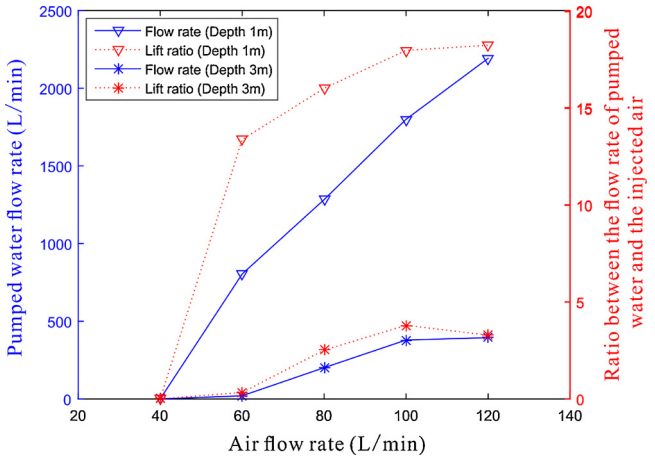

Fig. 9. Variations of pumped water volume flow rate and lift effectiveness at different submerged depths (Sea trial 1–6 and 1–9). The triangles and the axes stand for pumped water flow rate at submerged depths of 1 m and 3 m, respectively.

rate, i.e. 40 L/min, is required. As the air flow rate increases a little more, the water then begins to be pumped from the bottom to the upper outlet. However, in the lake experiments, the density difference is less than 1.6 kg/m^3, which is much smaller than that in the sea trial (see Fig. 4a and b). Therefore, the minimum air flow rate required to lift the water is relatively smaller and the bottom water can be pumped at even very low air flow rate in the lake experiments. Furthermore, the results show a common pattern of variation for both submerged depths that the pumped water flow rate increases with the increase of air flow rate. In addition the results also demonstrate that upwelling pipe deployed at shallower depth has a better performance than that deployed deeper. When the air flow rate is below 120 L/min, the maximum pumped water flow rates for submerged depth 1 m and 3 m are 2200 L/min and 400 L/min, respectively, and the maximum lift effectiveness for submerged depth 1 m and 3 m are 18 and 4, respectively. Though the data of pumped water flow rates presented in Figs. 8 and 9 are from different field experiments, they have similar trends increasing with the increase of air flow rate. Besides, the results from different experiments exhibit the same pattern that pumped water flow rate and lift effectiveness increase with the decrease of submerged depth. This effect of submerged depth is mainly related to the vertical distribution of density in the experiment site (See Fig. 4). In the experiments, the lower end of upwelling pipe was located within the pycnocline, therefore denser water was pumped to the surface when the upwelling pipe was deployed at a greater depth, and thus leading to a lower pumped water flow rate and lower lift effectiveness.

3.3. Effects of submergence ratio on pumped water flow rate

Submergence ratios of the field experiments are listed in Table A1 in the Appendix. Experiment results of sea trial 1–6 (SR = 0.375) and 1–10 (SR = 0.125) are compared in Fig. 10. It can be seen that the differences of lift effectiveness between the two pipes deployed with different submergence ratios (SR) are significant, and the maximum difference of lift effectiveness between them is about 10 at an air flow rate of 120 L/min. It seems that the pipe of 0.375 SR exhibits a higher efficiency over the pipe of 0.125 SR, not to mention that the hole size of nozzle used in the upwelling pipe deployed at 0.375 SR is larger than that deployed at 0.125 SR (See Table A1), which further confirms that the lift effectiveness increases with the increase of submergence ratio. This result is expected since increasing the submergence ratio indicates an increase in the interaction time between bubbles and the ambient water, and thus increasing the driving power of airlift pump.

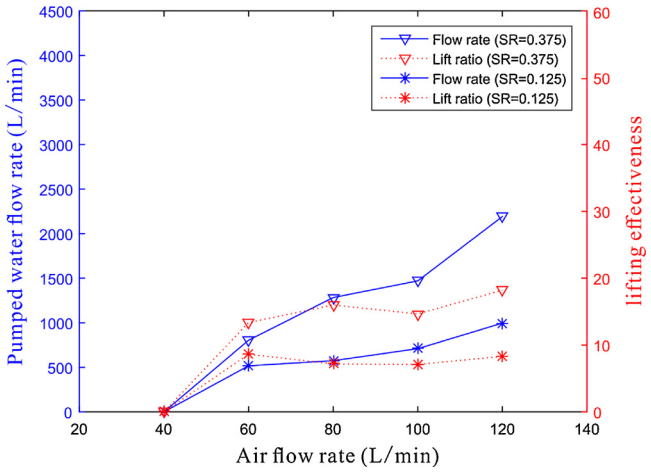

Fig. 10. Variations of pumped water volume flow rate and lift effectiveness at different submergence ratios in Sea trial 1–6 (SR = 0.375) and Sea trial 1–10 (SR = 0.125).

3.4. Effects of injection method on pumped water flow rate

3.4.1. Hole size

The effects of nozzles with different hole sizes are studied in the present study and the experiment results are presented in Figs. 11 and 12. Fig. 11 shows the experiment results of different nozzles from the sea trial, in which two kind of nozzles, P2 (hole size 1 mm) and P3 (hole size 0.5 mm), are compared here. It is evident that upwelling pipe equipped with nozzle P2 pumps more water than that equipped with nozzle P3 at the same air flow rate. The difference of pumped water flow rate between nozzle P2 and P3 is about 1500 L/min at a given air flow rate of 120 L/min, and the lift effectiveness of nozzle P2 is three times more than that of nozzle P3. The result in Fig. 11 preliminarily indicates the trend that pumped water flow rate increases with the increase of hole size.

Fig. 12 presents the experiment results of different nozzle sizes from lake experiment 1. In Fig. 12, two nozzles, R1and R4, are compared here. The hole sizes for nozzles R1 and R4 are 2 mm and 0.5 mm, respectively. Except for nozzle sizes, the other conditions for these two kind of nozzles are the same in the experiments. For both the nozzles in Fig. 12(a), the pumped water flow rate tends to fall on the same characteristic pattern increasing with the air flow rate rapidly, and after

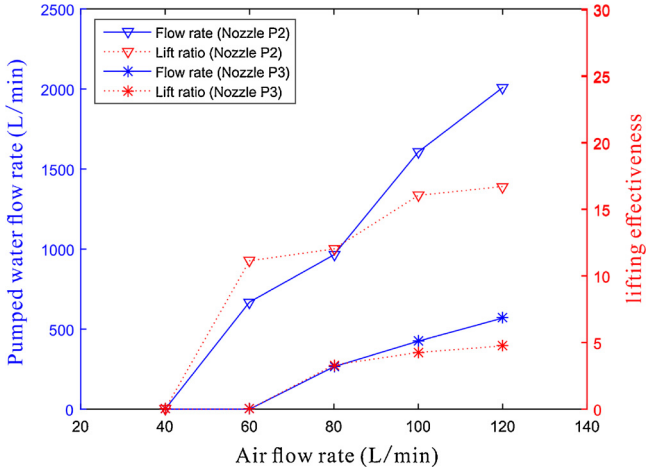

Fig. 11. Variations of pumped water volume flow rate and lift effectiveness of different hole sizes (Sea trial 1–3 and 1–12). The triangles and the axes stand for the experiment results of nozzles with hole diameter of 1 mm and 0.5 mm, respectively.

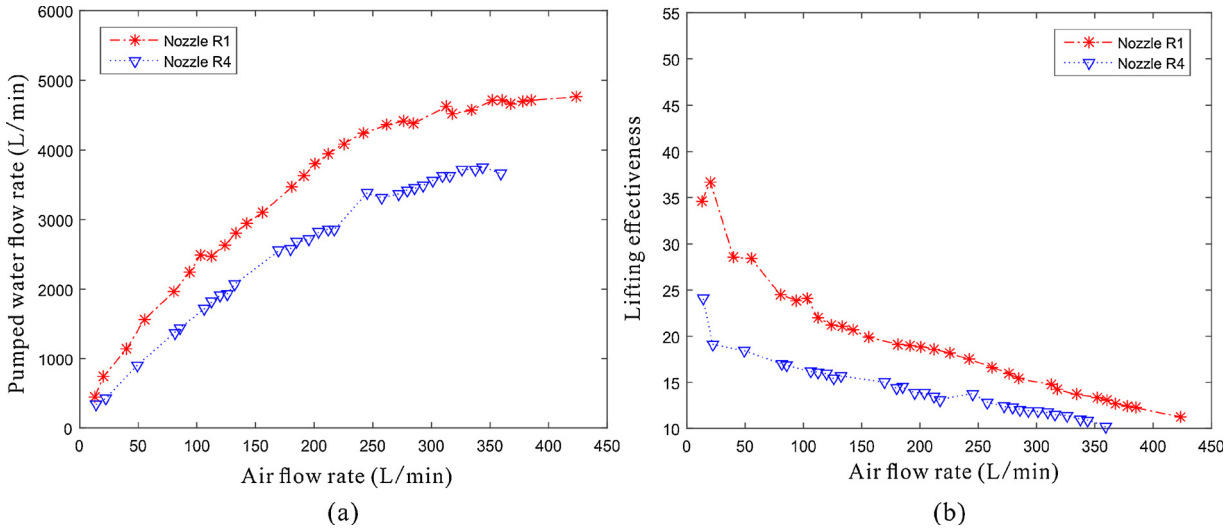

Fig. 12. Variations of pumped water volume flow rate and lift effectiveness of different hole sizes (Lake 1). The hole sizes of nozzle C1 and R1 are 2 mm, and the hole sizes of nozzle C2 and R4 are 0.5 mm.

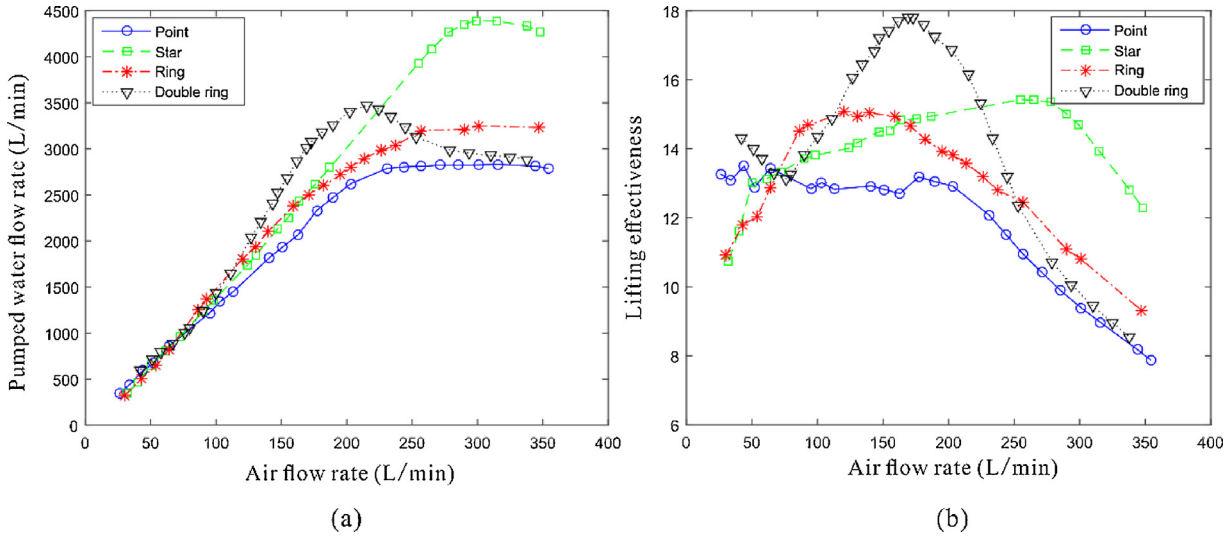

Fig. 13. Variations of pumped water volume flow rate and lift effectiveness of different nozzle shapes (Lake 2–4, 7, 9 and 11). The circles, squares, axes and triangles represent nozzle P1 (Point), S2 (Star), R2 (Ring) and D1 (Double ring), respectively.

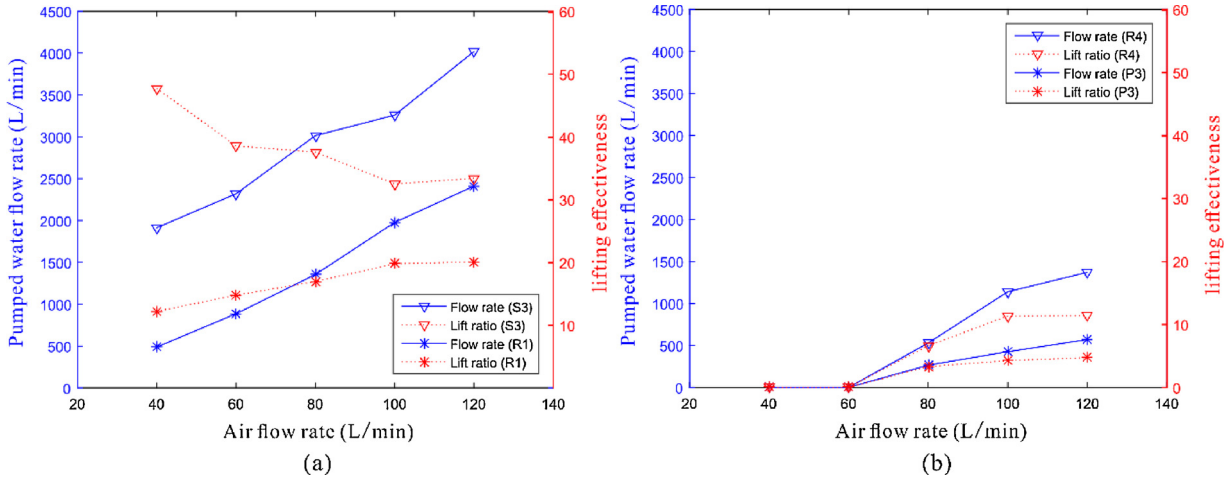

Fig. 14. Variations of pumped water volume flow rate and lift effectiveness of different nozzle shapes. (a) Triangles and axes represent nozzle S3 and R1, respectively (Sea trial 1–2 and 1–11); (b) Triangles and axes represent nozzle R4 and P3, respectively (Sea trial 1–5 and 1–12).

the air flow rate reaches about 250 L/min, the growth rate slows down. It is clear that nozzle R1 has a better performance than nozzle R4. The difference of pumped water flow rate between nozzle R1 and R4 is significant and it can reach about 25% at a given air flow rate of 350 L/min. The lift effectiveness in Fig. 12(b) also shares the same pattern varying with the air flow rate. It can be seen that the lift effectiveness decreases sharply at first, and then it slows down and tends to stay at a certain value. The explanation is that the cross-sectional area of upwelling pipe occupied by water volume decreases with the increase of air volume fraction, and thus the lift effectiveness would decrease to a very low value.

From Figs. 11 and 12, it can be concluded that the lift effectiveness of airlift pump increases with the increase of hole sizes on the nozzle. On the other hand, if the hole sizes on the nozzle are too large relative to the upwelling pipe, the lift effectiveness of the pump will decrease for not being operated in the bubbly-slug flow [23]. Therefore, an optimum hole size may be existed for upwelling pipe of a certain diameter.

3.4.2. Nozzle shape

Effects of different nozzle shapes on the performance of upwelling pipe are studied here, and the data from the lake experiment and sea trial are plotted in Figs. 13 and 14. Fig. 13 presents the experiment results of 4 different nozzle shapes (point, star, ring and double ring) from the lake experiment 2. It can be seen from Fig. 13(a) that almost all the different shapes of nozzles have the same tendency increasing with the air flow rate. As the air flow rate increases, the pumped water flow rate increases up to a certain maximum value, and after that it remains at the maximum value (point and ring) or begins to decrease (star and double ring). The lift effectiveness of 4 different nozzle shapes are presented in Fig. 13(b). It is clear that the results for different nozzle shapes almost indicate a common pattern of variation. The lift effectiveness increases with the increase of air flow rate to a maximum value, after that it decreases rapidly as the air flow rate keeps increasing. It can also be seen from Fig. 13(b) that there is no best nozzle for all the range of air flow rate. For air flow rate less than 75 L/min, nozzle of double ring shape pumps the most water among the four shapes. For air flow rate between 75 and 120 L/min, nozzle of ring shape is better even though the differences of lift effectiveness between these 4 shapes are within 2. When air flow rate ranges from 120 to 220 L/min, nozzle of double ring shape is clearly the best nozzle design and it has the highest maximum lift effectiveness of 18. While nozzle of point shape shows the worst performance with a maximum lift effectiveness of 13. For the rest of air flow rate range, the lift effectiveness of double ring decrease sharply and even becomes the same as the point shape. Nozzle of star shape then becomes the best nozzle for upwelling, and the differences of lift effectiveness between nozzle of star shape and the other nozzles are 5 on average. It can be seen that nozzle of a certain shape is not the best nozzle for all conditions, but on the whole, the best nozzle shape for upwelling is double ring and star when the air flow rate is less or more than 220 L/min, respectively.

Different shapes of nozzles (star, ring and point) are also studied in the sea trial and the experiment results are presented in Fig. 14, in which four sea trial experiments, 1–2(S3), 1-11(R1), 1–5(R4) and 1-12(P3) are selected and compared separately. Submerged depths for sear trial 1–2, 5 and 1–11, 12 are 1 m and 1.5 m, respectively. However, according to the vertical profile of density in sea trial (see Fig. 4c), the pipe length is 20 m, thus, the upwelling pipe sucks water from about 21 m and 21.5 m. Water densities at depth 21 m and 21.5 m are 1022.77 and 1022.81 kg/m^3, respectively. The density difference is about 0.04 kg/m^3, which has little influence on pumped water flow rate and can be negligible here. Therefore, submerged depths are assumed to be the same for these four experiments. Besides, the other conditions for these four experiments are the same, except for different hole sizes on these four nozzles, which are selected on purpose for the comparisons later. According to the effect of hole size on pumped water flow rate discussed in Section 3.4.1, nozzle with hole diameter 2 mm performs better than that with hole diameter 1 mm. While in Fig. 14(a), it is clear that the star shape nozzle S3 (1 mm holes) pumps more water and has higher lift effectiveness than the ring shape nozzle R1 (2 mm holes), and the difference of pumped water flow rate between these two nozzles is about 1700 L/min on average. This indicates that nozzle of star type performs better than that of ring type. In Fig. 14(b), it can be seen that nozzles R4 (0.5 mm holes) and P3 (0.5 mm holes) have the same pattern of variations with air flow rate. However, the nozzle R4 of ring shape pumps more water and has higher lift effectiveness than the nozzle of point shape. Therefore, the results in Fig. 14 indicate that the star shape is the best for nozzle designs among the three shapes, while the point shape is not recommended for nozzle designs, which is in accordance with the results of the lake experiments in Fig. 13.

4. Conclusions

In the present work, the effect of operating parameters and injection method on the performance of an airlift pump for artificial upwelling is investigated experimentally through two lake experiments and one open sea trial. Experiment results confirm that the airlift pump is an effective method for artificially upwelling deep, nutrient-rich water into the euphotic layer to stimulate the growth of phytoplankton. The results also show that the performance of airlift pump for artificial upwelling strongly depends on the operating parameters and injection method. The following conclusions can be deduced from the results:

(1) The upwelling lift effectiveness increases with the increase of the upwelling pipe diameter due to the reduction of fiction loss on the pipe inner wall. On the other hand, the pipe size should not be too large relative to nozzle size, otherwise M-shaped flow would occur in the pipe and reduce the efficiency. According to the experiment results in this study, a diameter of 1 m is recommended for upwelling pipe.
(2) The lift effectiveness of the airlift artificial upwelling is closely related to the submerged depth and submergence ratio of upwelling pipe. Reducing the submerged depth or increasing the submergence ratio leads to a higher pump lift effectiveness. On the contrary, increasing the submerged depth or reducing the submergence ratio will decrease the quantity of pumped water at a certain air flow rate.
(3) The lift effectiveness of the airlift artificial upwelling is also strongly dependent on the design of nozzle, including the overall shape and the hole size of nozzle. According to the results, there is no best nozzle for all the range of air flow rate investigated. The nozzle shape recommended for upwelling is double ring and star when the air flow rate is less or more than 220 L/min, respectively. In addition, increasing the hole size will also enhance the performance of airlift pump for artificial upwelling.
(4) The effect of submerged depth is mainly related to the vertical distribution of density in the experiment site. The denser water was pumped to the surface when the upwelling pipe was deployed at a greater depth, and thus leading to a lower pumped water flow rate and lower lift effectiveness.

Acknowledgments

This research is a contribution to the international IMBER project and is financially supported by the National Key R&D Program of China (2016YFA0601404), and the National Natural Science Foundation of China (No. 41406084 and No. 41776084).

Appendix A

See Tables A1 and A2

Table A1
List of experiment conditions.

Experiment	Nozzle	Pipe diameter (m)	Pipe length (m)	Submerged depth (m)	Injection depth (m)	Submergence ratio
Lake 1-1	R1	0.4	28.3	2.1	10.1	0.28
Lake 1-2	R4	0.4	28.3	2.1	10.1	0.28
Lake 2-1	P1	0.5	26	1.7	8.1	0.32
Lake 2-2	P3	0.5	26	0.7	7.1	0.32
Lake 2-3	P3	1	26	1.7	8.1	0.32
Lake 2-4	P1	1	26	1.7	8.1	0.32
Lake 2-5	S4	1	26	2.3	8.7	0.32
Lake 2-6	S4	1	26	0.15	6.55	0.32
Lake 2-7	S2	1	26	2	8.4	0.32
Lake 2-8	R4	1	26	2	8.4	0.32
Lake 2-9	R2	1	26	2	8.4	0.32
Lake 2-10	D2	1	26	2	8.4	0.32
Lake 2-11	D1	1	26	2	8.4	0.32
Lake 2-12	P1	1.5	26	2	8.4	0.32
Lake 2-13	D1	1.5	26	2	8.4	0.32
Lake 2-14	R2	1.5	26	2	8.4	0.32
Lake 2-15	S2	1.5	26	2	8.4	0.32
Lake 2-16	P1	2	26	2	8.4	0.32
Lake 2-17	D1	2	26	2	8.4	0.32
Lake 2-18	S2	2	26	2	8.4	0.32
Lake 2-19	R2	2	26	2	8.4	0.32
Sea trial 1-1	S4	0.4	20	1	3	0.125
Sea trial 1-2	S3	0.4	20	1	5	0.25
Sea trial 1-3	P2	0.4	20	1	7	0.375
Sea trial 1-4	R3	0.4	20	1	3	0.125
Sea trial 1-5	R4	0.4	20	1	5	0.25
Sea trial 1-6	S3	0.4	20	1	7	0.375
Sea trial 1-7	R3	0.4	20	3	5	0.125
Sea trial 1-8	R4	0.4	20	3	6	0.25
Sea trial 1-9	S3	0.4	20	3	9	0.375
Sea trial 1-10	S1	0.4	20	1.5	3.5	0.125
Sea trial 1-11	R1	0.4	20	1.5	5.5	0.25
Sea trial 1-12	P3	0.4	20	1.5	7.5	0.375

Table A2
List of experiment results.

Experiment	Air volume flow rate (L/min) Pumped water volume flow rate (L/min)											
Lake 1-1	13	55	94	133	156	191	225	262	285	334	378	424
	450	1565	2247	2806	3102	3630	4092	4361	4384	4570	4699	4763
Lake 1-2	14	49	86	113	132	170	204	245	279	301	326	359
	337	904	1450	1822	2071	2555	2820	3382	3423	3565	3717	3663
Lake 2-1	14	21	53	60	66	106	115	122	197	207	216	227
	188	261	442	485	516	756	808	858	1333	1389	1441	1502
Lake 2-2	47	73	99	123	154	187	206	227	250	330	357	387
	1404	1821	2234	2596	1894	2949	2976	2959	2966	2749	2618	2525
Lake 2-3	47	67	105	124	147	172	206	222	250	279	308	322
	664	1083	1574	1821	2041	2287	2623	2671	2731	2785	2809	2817
Lake 2-4	52	64	103	113	151	177	203	231	257	271	301	344
	670	860	1341	1449	1936	2333	2623	2789	2810	2824	2827	2813
Lake 2-5	45	75	104	128	152	180	194	232	252	269	284	296
	765	1360	1916	2161	2414	2617	2689	2846	2848	2840	2838	2867
Lake 2-6	47	73	97	128	152	170	205	224	242	282	307	329
	856	1743	2600	3467	3906	4233	4431	4511	4547	4526	4659	4691
Lake 2-7	50	72	98	124	147	176	187	255	265	278	299	338
	650	960	1353	1738	2131	2619	2795	3935	4084	4268	4394	4332
Lake 2-8	48	77	100	128	151	173	201	227	250	275	301	320
	380	812	1252	2002	2388	2498	2683	2829	2873	2845	2789	2680
Lake 2-9	54	86	93	120	140	171	195	226	257	290	301	347
	650	1249	1365	1808	2104	2505	2716	2984	3200	3213	3251	3232
Lake 2-10	47	71	100	132	149	180	200	222	247	271	301	324
	576	871	1870	2937	3121	3105	2995	2906	2809	2795	2792	2788
Lake 2-11	51	76	100	127	147	173	202	224	253	279	294	325
	713	998	1436	2038	2529	3079	3409	3436	3126	2989	2952	2912

(continued on next page)

Table A2 (*continued*)

Experiment	Air volume flow rate (L/min) Pumped water volume flow rate (L/min)											
Lake 2-12	48	82	105	131	153	174	203	232	248	269	311	338
	318	475	589	736	846	990	1126	1337	1375	1473	1706	1658
Lake 2-13	51	73	101	124	148	173	200	228	250	277	301	331
	197	277	344	415	490	568	658	736	872	945	940	899
Lake 2-14	49	79	100	127	150	171	200	229	251	275	299	324
	187	258	321	411	489	562	649	715	760	778	759	743
Lake 2-15	52	75	100	130	150	177	198	228	248	275	300	323
	233	314	415	517	586	658	707	759	796	843	321	936
Lake 2-16	40	68	91	121	154	171	194	226	253	273	307	339
	301	331	352	376	404	414	422	437	444	450	421	366
Lake 2-17	55	75	99	123	150	176	200	225	252	274	300	325
	188	269	339	389	429	446	458	469	456	455	431	415
Lake 2-18	48	72	100	125	151	177	200	223	253	274	298	320
	311	366	431	494	553	580	591	574	540	500	460	436
Lake 2-19	47	67	100	125	149	180	199	223	250	275	301	331
	180	234	268	301	331	361	374	391	403	406	403	395
Sea trial 1-1	40	60	80	100	120	—	—	—	—	—	—	—
	1470	2153	2318	2740	3173	—	—	—	—	—	—	—
Sea trial 1-2	40	60	80	100	120	—	—	—	—	—	—	—
	1913	2318	3014	3258	4019	—	—	—	—	—	—	—
Sea trial 1-3	40	60	80	100	120	—	—	—	—	—	—	—
	0	670	965	1608	2010	—	—	—	—	—	—	—
Sea trial 1-4	40	60	80	100	120	—	—	—	—	—	—	—
	0	0	0	0	913	—	—	—	—	—	—	—
Sea trial 1-5	40	60	80	100	120	—	—	—	—	—	—	—
	0	0	529	1137	1370	—	—	—	—	—	—	—
Sea trial 1-6	40	60	80	100	120	—	—	—	—	—	—	—
	804	1283	1800	2192	—	—	—	—	—	—	—	—
Sea trial 1-7	40	60	80	100	120	—	—	—	—	—	—	—
	—	—	—	—	—	—	—	—	—	—	—	—
Sea trial 1-8	40	60	80	100	120	—	—	—	—	—	—	—
	0	0	0	0	1340	—	—	—	—	—	—	—
Sea trial 1-9	40	60	80	100	120	—	—	—	—	—	—	—
	0	0	201	379	394	—	—	—	—	—	—	—
Sea trial 1-10	40	60	80	100	120	—	—	—	—	—	—	—
	0	517	574	709	996	—	—	—	—	—	—	—
Sea trial 1-11	40	60	80	100	120	—	—	—	—	—	—	—
	488	887	1355	1977	2412	—	—	—	—	—	—	—
Sea trial 1-12	40	60	80	100	120	—	—	—	—	—	—	—
	0	0	265	425	569	—	—	—	—	—	—	—

References

[1] D. Tanner, Ocean thermal energy conversion: current overview and future outlook, Renew. Energy 6 (1995) 367–373.

[2] Y. Pan, W. Fan, T.H. Huang, S.L. Wang, C.T. Chen, Evaluation of the sinks and sources of atmospheric CO2 by artificial upwelling, Sci. Total Environ. 511 (2015) 692–702.

[3] B. Kirke, Enhancing fish stocks with wave-powered artificial upwelling, Ocean Coast. Manage. 46 (2003) 901–915.

[4] W. Fan, J. Chen, Y. Pan, H. Huang, C.-T. Arthur Chen, Y. Chen, Experimental study on the performance of an air-lift pump for artificial upwelling, Ocean Eng. 59 (2013) 47–57.

[5] S. Maruyama, K. Tsubaki, K. Taira, S. Sakai, Artificial upwelling of deep seawater using the perpetual salt fountain for cultivation of ocean desert, J. Oceanogr. 60 (2004) 563–568.

[6] H. Stommel, A.B. Arons, D. Blanchard, An oceanographical curiosity: the perpetual salt fountain, Deep Sea Res. (1953) 3 (1956) 152–153.

[7] K. Tsubaki, S. Maruyama, A. Komiya, H. Mitsugashira, Continuous measurement of an artificial upwelling of deep sea water induced by the perpetual salt fountain, Deep Sea Res. Part I: Oceanogr. Res. Papers 54 (2007) 75–84.

[8] J.D. Isaacs, D. Castel, G.L. Wick, Utilization of the energy in ocean waves, Ocean Eng. 3 (1976) 175–187.

[9] C. Liu, Research on artificial upwelling and mixing at the university of Hawaii at Manoa, IOA Newsletter 10 (1999) 1–8.

[10] K.E. Kenyon, Upwelling by a wave pump, J. Oceanogr. 63 (2007) 327–331.

[11] N.-K. Liang, H.-K. Peng, A study of air-lift artificial upwelling, Ocean Eng. 32 (2005) 731–745.

[12] N. Williamson, A. Komiya, S. Maruyama, M. Behnia, S.W. Armfield, Nutrient transport from an artificial upwelling of deep sea water, J. Oceanogr. 65 (2009) 349–359.

[13] C.C. Liu, Q. Jin, Artificial upwelling in regular and random waves, Ocean Eng. 22 (1995) 337–350.

[14] A. Di Gerlando, G. Foglia, M. Iacchetti, R. Perini, F. Gatelli, L. Armellin, Torque and losses in the metallic shell of a dual mechanical port PM electrical machine, for dangerous fluid pumps, Electrical Machines (ICEM), 2010 XIX International Conference on: IEEE, (2010), pp. 1–6.

[15] S.H. Kim, C.H. Sohn, J.Y. Hwang, Effects of tube diameter and submergence ratio on bubble pattern and performance of air-lift pump, Int. J. Multiphas Flow 58 (2014) 195–204.

[16] K. Pougatch, M. Salcudean, Numerical modelling of deep sea air-lift, Ocean Eng. 35 (2008) 1173–1182.

[17] W. Fan, Y. Pan, C.C. Liu, J.C. Wiltshire, A.C. Chen-Tung, Y. Chen, Hydrodynamic design of deep ocean water discharge for the creation of a nutrient-rich plume in the South China Sea, Ocean Eng. 108 (2015) 356–368.

[18] F. De Cachard, J. Delhaye, A slugh-churn flow model for small-diameter airlift pumps, Int. J. Multiphas Flow 22 (1996) 627–649.

[19] F. De Cachard, J. Delhaye, Stability of small diameter airlift pumps, Int. J. Multiphas Flow 24 (1998) 17–34.

[20] M. Khalil, K. Elshorbagy, S. Kassab, R. Fahmy, Effect of air injection method on the performance of an air lift pump, Int. J. Heat Fluid Flow 20 (1999) 598–604.

[21] W. Ahmed, A. Aman, H. Badr, A. Al-Qutub, Air injection methods: the key to a better performance of airlift pumps, Exp. Therm. Fluid Sci. 70 (2016) 354–365.

[22] J. Yang, D. Zhang, Y. Chen, W. Fan, H. Liang, M. Tan, Feasibility analysis and trial of air-lift artificial upwelling powered by hybrid energy system, Ocean Eng. 129 (2017) 520–528.

[23] P. Hanafizadeh, M. Saidi, A. Karimi, A. Zamiri, Effect of bubble size and angle of tapering upriser pipe on the performance of airlift pumps, Part. Sci. Technol. 28 (2010) 332–347.